# RSC Advances

This article can be cited before page numbers have been issued, to do this please use: S. Peril, A. Raj, M. Doble and A. Sen, *RSC Adv.*, 2016, DOI: 10.1039/C6RA09099K.

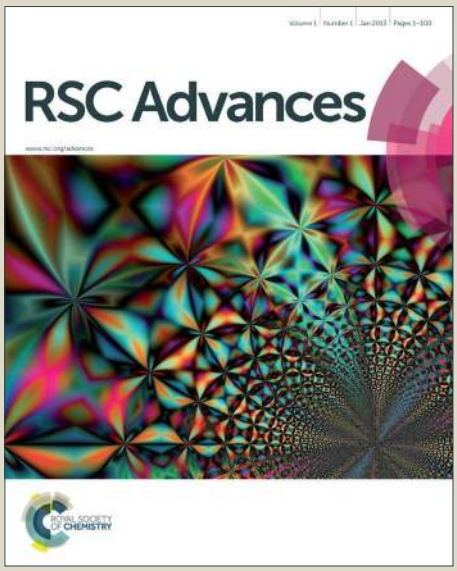




ROYAL SOCIETY OF CHEMISTRY

www.rsc.org/advances

View Article Online
DOI: 10.1039/C6RA09099K



# Characterization and sorting of cells based on stiffness contrast in a microfluidic channel

P. Sajeesh[1], A. Raj[1], M. Doble[2], A. K. Sen[1,*]

[1]*Department of Mechanical Engineering, Indian Institute of Technology Madras, Chennai-600036, India*
[2]*Department of Biotechnology, Indian Institute of Technology Madras, Chennai-600036, India*

[*]Author to whom correspondence should be addressed. Email: ashis@iitm.ac.in



## Abstract

This paper reports the characterization and sorting of cells based on stiffness contrast. Cell stiffness is characterized in terms of elastic modulus, deformability index and hydrodynamic resistance. For different cell types, elastic modulus is measured using nanoindentation experiments on AFM and deformability index of cells is measured by hydrodynamic stretching of the cells in a flow focusing microchannel device. Hydrodynamic resistance of cells is obtained by measuring the excess pressure drop across a segment of a microchannel and correlated with cell size $\rho_c$and elastic modulus $E_c^*$ using a large set of experimental data. The highly-invasive malignant breast cancer cells MDA MB 231, non-invasive malignant breast cancer cells MCF 7, human promyelocytic leukaemia cells HL 60 and the cervical cancer cells HeLa are considered in the present study. A microfluidic device with focusing and spacing control for stiffness based sorting of cells is designed and fabricated. Experiments are performed to demonstrate cell sorting and charcterize the device performance in terms of sorting efficiency, which was found to depend on the stiffness contrast. The proposed device has potential to be used as a lab on chip diagnostic tool for sorting of diseased cells from healthy cells based on stiffness contrast.

## 1. Introduction

Lab on Chip (LOC) devices are widely used in healthcare, research and industry for the sorting of micron sized objects such as cells, droplets and particles into distinct populations[1–3]. The variations in the physical properties of cells viz. size, shape, stiffness and optical properties can be used as biomarkers to detect various diseases including malaria, sickle cell anaemia, cancer and HIV[4–8]. The size and stiffness of healthy cells get modified in case of diseases though abnormalities in cytoskeleton structure. For example, when Red Blood Cells (RBCs) are infected with malarial parasites, the RBCs tend to block the blood capillaries due to increased stiffness[9,10]. In sickle cell anaemia, due to the aggregation and polymerization of haemoglobin molecules, the rigidity of RBCs increases[11–13]. The size of a sickle cell is smaller and has different morphology as compared to a healthy cell. Similarly, epithelial cancer cells MCF 7 have larger size and higher deformability as compared to healthy cells MCF 10A[14]. The average elastic modulus of lymphocytes is two-fold higher than that of Jukart cells[15]. This increased stiffness is because of the change in the cytoskeletal structure from an organized state to an irregular state. Also, stiffness of RBCs decreases due to hemodynamic alterations and micro-circulatory disturbances during the course of Systemic Inflammatory Response Syndrome (SIRS) especially sepsis[16].

Invasiveness of a cancer cell can also be related with its stiffness. Highly invasive malignant human breast cancer cell line MDA MB 231 has lower Young's modulus than that of non-invasive malignant cancer cell line MCF 7, which is further lower than that of benign cells MCF 10A[17]. Also, it is reported that human myeloid HL 60 cells are eighteen-times stiffer than lymphoid leukaemia Jurkat cells and six-times stiffer than neutrophils[18]. Atomic Force Microscopy (AFM) studies have shown that Young's modulus of HeLa cells is much higher than most of the other cancer cell lines[19]. Although, in most cases, the healthy cells are stiffer as compared to the breast and lung cancer cells, lymphocytes from patients with chronic lymphocytic leukaemia have higher stiffness as compared to those from healthy donors[20]. Certain studies emphasise that cancer cells become slightly stiffer as they proceed towards the final metastatic state[21]. Thus, size and stiffness of cells can be used as biomarkers for the detection of different diseases and their invasiveness.

Entry and transit time[22] required for a cell to pass through a constriction in a microchannel can be related with its stiffness, but such parameters get affected by the size and the frictional properties of the cells and the channel wall[23]. Cells with more metastatic potential show faster entry and transit velocities compared to cells with lower potential, due to both increased deformability and reduced friction. Although, micropipette aspiration[24] is one of the established methods to evaluate surface tension (or cortical tension) of cell membrane as a deformability parameter, stiffness of entire cell (including membrane, nucleus and cytoskeleton) can be indicated by its Young's modulus. In AFM studies, nano-indentation curves, which are generated by vertical 'tip-cell' interaction without any lateral movement of the tip, are analysed to estimate the Young's modulus of cell lines[25]. A comparison of the Young's modulus values of different cell lines from AFM measurements reported in different literatures may not provide an accurate comparison of their stiffness since the values strongly depend on the loading rate of AFM probe[26], the method by which the cells are immobilized on a substrate and the depth of indentation on the cells. Thus we perform AFM measurements on different cells by keeping all the above parameters fixed. Although previous works showed that the stiffness of a cell is independent of its cell size[27], recently it is reported that there exist an inverse relationship between the size and deformability of cells[28] i.e. smaller cells

View Article Online
DOI: 10.1039/C6RA09099K




show higher deformability than the larger cells. In order to isolate the effect of cell size from the measured stiffness, we have performed indentation experiments on cells of a fixed size for the different cell lines.

A detailed review of the various active and passive techniques that are used for sorting of microparticles is reported in literature[2,3]. In point of care LOC devices, passive sorting mechanisms are preferred in order to overcome the limitations of the active methods in terms of process and fabrication complexity and cost. Various passive separation and sorting methods[29] including pinched flow fractionation (PFF), cross flow filtration, hydrodynamic filtration have been used for the sorting of droplets and cells based on size. However, such methods cannot be used for the sorting of cells based on stiffness. Although, Deterministic Lateral Displacement (DLD) devices can be used to sort cells based on size, shape and deformability[30], the fabrication of closely spaced posts inside microchannels is challenging and there is higher chance of clogging at higher sample concentrations. Inertial focussing[31] method is also used for sorting of cells based on stiffness in which the cells are focussed at different lateral positions inside the microchannel owing to the balance between deformability induced lift forces (which is function of cell stiffness)[32], shear induced and wall induced lift forces. The sorting efficiency can be affected by the change in the shape of the cells due to the variation in deformability induced lift force acting on the cells[33]. Hydrodynamic resistance offered by objects inside a microchannel can be considered as a biomarker for cells of different size and deformability[34,35]. Here, we report a passive sorting technique that has the advantages of both hydrodynamic filtration (reduced clogging) and hydrodynamic resistance[36] (stiffness as a marker) methods. The present technique requires much smaller device foot print as compared to that required in case of hydrodynamic filtration. Focusing and spacing control modules used in the proposed device can handle the higher sample concentrations to provide high throughput.

In this work, we report characterization and sorting of cells based on stiffness contrast. First, materials and methods used in the experiments are detailed. A protocol for measuring the Young's modulus of cells using nanoindentation experiment on AFM is enumerated. Stiffness of cells is further quantified with the hydrodynamic stretching and deformability index (D.I). Further, the hydrodynamic resistance offered by various cell lines inside the microchannel were measured and correlated with cell size and stiffness. Next, the details of the device layout and operating principle are described. Finally, experimental results for sorting of different types of cells and the corresponding sorting efficiency are presented.

## 2. Materials and methods

To demonstrate sorting of cells based on stiffness contrast, samples of different cell lines of same size but different stiffness were used. To characterize the stiffness of different cell lines, cervical cancer cells HeLa, metastatic breast cancer cells MDA MB 231, non-metastatic breast cancer cells MCF 7 and human promyelocytic leukemia cells HL60 cells of same size were selected. The protocol for culturing HL 60 cells and sorting cells of particular size using Fluorescent Activated Cell Sorting (FACS Aria III, BD biosciences, USA) are reported in our earlier work[36]. The protocol used for culturing the other cell lines and tagging (with dye) are provided in the Supplementary Information S.1. For sorting cells of a particular size, polystyrene bead (Sigma Aldrich, Bangalore) of the same size was used as the standard for calibration. The size variation of sorted cells in a sample is ±1 μm.

## 3. AFM protocol and data analysis

### 3.1 Cell immobilization

It is reported in literature that of cells cultured on a glass slide show an increased in stiffness during AFM measurements as compared to their actual stiffness values[37]. This is because; the fibroblast tries to stiffen the cytoskeleton structure of the cells to match its stiffness to that of the substrate on which the cells are cultured. So for the present AFM studies, cells were immobilized on Poly-L-Lysine coated glass slides for preventing artificial stiffening of the cell lines (refer Fig. S1 (a)). The protocol used for the cell immobilization and the images of the immobilized cell (HL 60 cell) on glass slide using Poly-L-Lysine is provided in the Supplementary Information S.2.

### 3.2 AFM probe

In order to measure force versus indentation characteristics for accurate prediction of Young's modulus of cells, stiffness of the cantilever probe should be comparable with that of the cell line. A colloidal probe CP-CONT-BSG (Nanoandmore Gmbh, Germany) with polystyrene bead of 10 $\mu m$ at the tip, having stiffness value of 0.045 N/m, was used. Moderate indentations on the cell lines (approx. 1000 nm) enabled us to obtain the precise Young's modulus of the cell lines, even in situations in which the accurate contact point was missed by few ten nanometres and force indentation curves have higher noise level[38]. Further details on the selection of the cantilever probe and SEM image of the AFM colloidal probe used in our studies are provided in Supplementary Information (refer Fig. S1(b)).

### 3.3 AFM nanoindentation experiments

Force versus indentation experiments were performed on contact force mapping mode using Confocal Raman Microscope (CRM-Alpha300 S, WiTec GmbH, Germany). Since the measurement of Young's modulus of a cell can also get influenced by the presence of the neighbouring cells during the indentation experiments[21], in the present studies, indentation experiments were performed on isolated cells to avoid this micro environment effect. Energy delivered by the indenter into the cell is not completely given back by cell due to the viscous dissipation. The viscous relaxation time scale

View Article Online
DOI: 10.1039/C6RA09099K





varies depending upon the applied loading rate during the nanoindentation experiment. Higher is the loading rate, smaller is the indentation on the cell at a given force, which leads to a higher apparent stiffness[39]. However at lower loading rate, indentation time exceeds the relaxation time scale, which allows the cell to undergo reorganization leading to lower apparent stiffness. An appropriate loading rate should be selected for reducing both these effects. Various cells characterized by nanoindentation experiment have different relaxation times owing to the size of nucleus, composition of cytoskeleton and cytoplasm[40]. Since the medium used around the cell in the nanoindentation experiment is air (not liquid) viscous dissipation losses are minimum and the time scales are almost of the same order. Moreover the indentation is performed using the colloidal probe (instead of pyramidal probe) with a sphere of diameter of 10 $\mu m$ at the tip of the probe. This reduces the effect of reorganization of cell structure during the nanoindentation experiments[41]. It is also reported in literature that measured Young's modulus is independent of the loading rate when the indentation experiments are performed at a loading rate < 400 nm/s[26]. Similarly, smaller loading rate eliminates the indentation produced by the acceleration of the AFM tip and thus nullifies hydrodynamic effects on measured values[42]. So we performed all the nanoindentation experiments at a loading rate 400 nm/s to compare stiffness of different cell lines. The voltage sensed during the nano-indentation experiments is converted to the corresponding deflection $d_c$ by multiplying output voltage $v$ with the sensitivity of the cantilever probe. Sensitivity of the probe is found out using force-indentation study performed on solid samples with known stiffness values. Silicon substrates were used for the sensitivity calibration of the AFM probes and the sensitivity of the probe used for the present study was measured to be 1530 nm/V.

In nanoindentation experiments, loading curve provides information regarding the repulsive or attractive forces between colloidal probe and sample. When probe is in contact with cell, as AFM stage proceeds up, probe deflects until equilibrium between elastic force and probe-cell interaction force is achieved so the mechanical properties of cell can be measured. During loading, deflection of probe cantilever and the corresponding output voltage suddenly increases at the contact point, which further continues to increase rapidly with increase in the indentation of the tip into the cell, as shown in Fig. 1. During unloading, when the cantilever is withdrawn from the cell, the deflection of the probe and hence the corresponding output voltage decreases. The unloading curve gives information about adhesion forces, existence of tethers and possible molecular unfolding events[40]. There are two non-contact regions: jump-to-contact in the loading curve and the jump-off-contact in the unloading curve. During loading, when the distance between the probe and cell goes below 13 Aº and the force gradient is higher than the effective constant of the cantilever, position of the cantilever becomes unstable and hence it jumps on the cell surface irrespective of the stiffness of the probe[39]. During unloading, when the elastic constant of the probe is larger than the gradient of the adhesive forces in the unloading curve, jump-off-contact occurs. In usual force-indentation analysis, jump-to-contact can be neglected but the jump-off-contact is considered in which the pull off force is of the order of few nN[39]. This is observed as a sudden dip in the deflection $d_c$ versus piezo position $z$ curve during the unloading process, as depicted in Fig. 1.

The difference between the loading and unloading curves indicate hysteresis which represents the viscous dissipation of energy into the cell. Hydrodynamic drag acting on the probe is the main reason for the hysteresis, if the indentation is performed in a liquid medium[40]. This viscous drag pulls the probe upward during the loading experiment and bends downward when the probe is unloaded from the cell. Adhesion force between the cell and the probe during the unloading experiments and cell viscosity are the sources of the hysteresis indentation experiments with living cells[41]. Friction between the cell and the probe during the contact region of the loading and unloading curve can also lead to hysteresis[39]. Hysteresis can be evaluated experimentally and numerically by taking the difference between the areas of the loading and unloading curves[43]. Hysteresis is proportional to the loading rate of the probe into the cell and can be reduced by lowering the loading rate. The load versus indentation experiments were performed at least thrice on a particular cell line, in which each indentation experiment is performed within a time period of 40 s. Measurements were performed on at least 20 cells for each cell line to determine the Young's modulus. All indentation experiments were performed within a time period of 2 h after the cell immobilization step to ensure that the cells stay viable during the measurements. The deflection $d_c$ versus piezo position $z$ data obtained during each indentation experiment (shown in Fig. 1) was then analysed using custom made MATLAB GUI AFM TOOL (Supplementary Information S.4) for evaluating the Young's modulus.

A custom made MATLAB code was developed to identify the precise contact point and fit the data for evaluating the Young's modulus of cells. A Graphical user interface (GUI) was developed in MATLAB for the data analysis which is provided in the Supplementary Information (Fig. S2). Piezo positions of the cantilever ($z$), deflection of the cantilever $d_c$ during the AFM experiments, maximum indentation range, radius of the spherical tip $R_t$ and stiffness of the cantilever ($k$) are the inputs that are entered into the GUI "AFMTOOL". The code plots the piezo position $z$ versus deflection $d_c$ curve, and locate the contact point $(z_0, d_0)$, which is indicated by a red circle on the plot, shown in Fig. S2 in Supplementary Information. From the identified contact point, the code automatically plots the indentation $I_d$ versus relative deflection $\delta_c$ profile for that particular cell indentation experiment. Finally, this profile is fitted with the Hertzian model [44] to provide the Young's modulus of the cell with a specified $R^2$ value of the fitting, as shown in Fig. S2. Further details regarding the AFM data analysis is provided as Supplementary Information section S.4.

View Article Online
DOI: 10.1039/C6RA09099K




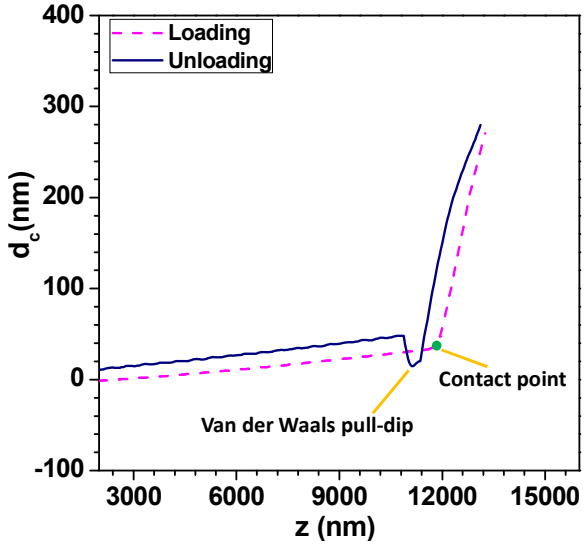


**Fig. 1** Deflection $d_c$ versus piezo position $z$ curve obtained from AFM nano-indentation experiments on HL 60 cell line of size 25 µm at a loading rate of 400 nm/s, identified contact point and the Van der Waals pull-dip are marked on the curve.

## 4. Sorting device description and principle

The microfluidic device for the sorting of cells based on their stiffness contrast is shown in Fig. 2(a). Earlier, we demonstrated the use of the device for size based sorting of droplets and cells[36]. Here we explain the device principle for sorting of objects based on stiffness contrast. The device has two modules: focusing and spacing control module and sorting module. The focusing and spacing control module in the device focuses the objects present in a sample onto one of the side walls of a channel with controlled spacing between them using a sheath fluid. A detailed theoretical and experimental description of the focusing and spacing control module is reported earlier[36]. In the sorting module, the main channel splits into straight and side branch channels with the flow into these two channels separated by a "dividing streamline". The width of the fluid stream from dividing stream line from the side wall is called the "critical stream width $w$". A sensing channel and a bypass channel in the sorting module control the shifting of the dividing streamline depending on the deformability of the objects. For the stiffness based sorting, in the absence of any object in the sensing channel, the initial critical stream width $w_0$ depends on the initial flow rate ratio $r_i$ (i.e. ratio of flow rates in the straight branch $Q_{st}$ to the side branch $Q_{si}$). For fixed size of the object $r_0$, the instantaneous flow rate ratio $r$ and hence the instantaneous critical stream width $w$ vary depending on the object stiffness, which in turn depends on the Young's modulus $E_c$. The shifting of "dividing streamline" (i.e. the streamline that separates the flow streams entering the two branch channels) and hence the critical stream width $w$ depends on the size and stiffness of the objects that arrive at the sensing channel. If the size ratio of the objects to be sorted is kept fixed, then the change in critical stream width $w$ is mainly governed by the Young's modulus $E_c$. The Young's modulus of a cell $E_c$ is non-dimensionalized with the maximum shear stress acting on the cell inside the channel, which gives $E_c^* = \frac{E_c H}{2\mu u_{\max}}$, where $u_{max}$ is the maximum velocity of sample inside microchannel, $\mu$ is the viscosity of the medium, in which the cells are suspended and $H$ is the channel height.

A schematic of the variation of the instantaneous critical stream width $w$ as a function of nondimensional Young's modulus $E_c^*$ is presented in Fig. 2(b). Initial critical stream width $w_0$ can be controlled by adjusting the flow rate ratio of the side-to-straight channel $Q_{si}/Q_{st}$. If the Young's modulus of a cell $E_c^*$ that arrives at the sensing channel is higher, it offers higher resistance and thus the instantaneous critical stream width $w$ decreases. For a certain Young's modulus value of a cell line, the size of the object $r_0$ and the instantaneous critical stream width $w$ are equal, which is known as the "threshold Young's modulus $E_{ct}^*$". Thus, for a fixed side-to-straight channel flow rate ratio $Q_{si}/Q_{st}$, the cells of stiffness lower than the threshold Young's modulus (i.e. $E_{cd}^* < E_{ct}^*$) can be sorted from that of stiffness higher than the threshold Young's modulus i.e.$E_{cs}^* < E_{ct}^*$. When an object of lower stiffness enters the sensing channel, due to lower resistance change[45], there is a smaller shift in the critical stream width $w$. However, when an object of higher stiffness enters the sensing channel, due to higher resistance change[45], there is a larger shift in the critical stream width $w$. In case of objects of lower stiffness, the instantaneous critical stream width is less than the size of the object i.e. $w_{de} < r_0$, thus such objects are sorted into the side branch channel (Fig. 2(c)). On the other hand, for objects of higher stiffness, the instantaneous critical stream width is more than the size of the object i.e.$w_{st} < r_0$, thus such objects get sorted into the straight branch channel (Fig. 2(d).

View Article Online
DOI: 10.1039/C6RA09099K





The proposed technique requires that the objects be focused onto a side wall and enter the sensing channel single-file, which is ensured by using a sheath fluid in the focusing and spacing control module. The focusing and spacing control module further helps in improving the sorting efficiency of the device owing to the higher hydrodynamic stretching of objects of lower stiffness. When objects of lower stiffness are focused onto a side wall using a sheath fluid, such objects undergo hydrodynamic stretching (refer Fig. 2(c)). Thus the effective radius of the objects (distance from the centre of mass of object to side wall) is further reduced as compared to the undeformed radius $r_0$ of the objects. This further ensures that an object of lower stiffness attains a smaller effective radius $r_0$ than the critical stream width $w_{de}$ and thus is sorted to the side branch. On the other hand, when a stiffer object is focused to the side wall, the hydrodynamic stretching of such an object is negligible and thus their effective radius remains unchanged (refer Fig. 2(d)). This keeps the critical stream width $w_{st}$ less than effective radius $r_0$ and thus the stiffer object will continue its path along the straight branch. In all the cases, the bypass flow rate $Q_b$ is very small compared to the main channel flow rate $Q_t$ such that the critical stream width at bypass channel $w_b$ is much smaller as compared to the object radius which prevents the objects from entering the bypass channel.

To ensure the device operation, the dynamic effects of the shifting of streamline due to the presence of an object in the sensing channel needs to be analysed. The inertial time scale $\tau_i$ required for the fluid to change from one steady state to another can be obtained from the following expression[46],

$$\tau_i = \frac{\rho_f H_0^2}{\mu} \quad (1)$$

where $\rho_f$ is the fluid density, $H_0$ is the channel height (smallest length scale in the channel), and $\mu$ is the dynamic viscosity of the sample fluid. Considering the dimensions of the channel and the properties of the fluids used in our experiments, the inertial time scale is found to be of the order of 10 µs. When a deformable object enters into the sensing channel, the dividing streamline is shifted from its original position to a new position, which is determined by the resistance offered by the object in the sensing channel. The shifting of the dividing streamline takes place over a time period equal to the inertial time scale. A deformable object remain in the sensing channel over a time scale which depends on the total flow rate of the sample and sheath fluids used in our experiments. The shifted dividing streamline position continues to be the same as long as the object remains in the sensing channel. The residence time of the object in the sensing channel in all our experiments is ~ms, which is much larger than the inertial time scale. Since the residence time of the objects is more than the inertial time scale, it provides adequate time for the shift in the streamline to take place and the objects have sufficient time to respond to the change in the critical stream width.

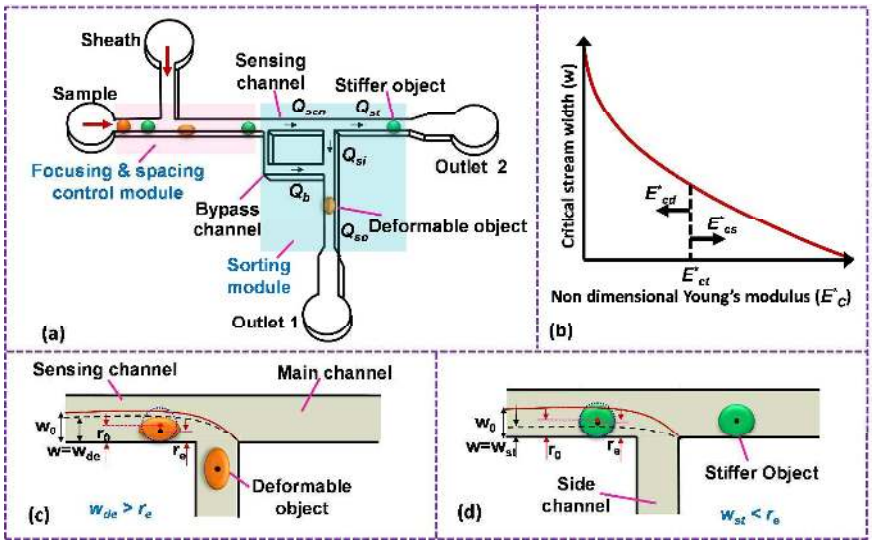


**Fig.2** Schematic of the (a) stiffness-based sorting device (b) variation of instantaneous critical stream width $w$ with Young's modulus $E_c^*$ (c) deformable objects of effective radius $r_e$< critical stream width $w_{de}$ are sorted to the side branch (d) stiffer object of effective radius $r_e$> the critical stream width $w_{st}$ continue to flow along the main channel.

View Article Online
DOI: 10.1039/C6RA09099K




## 5. Results and Discussion

### 5.1 Comparison of the Young's modulus of different cell lines

The relative deflection $\delta_c$ versus indentation $I_d$ data for different cell lines, obtained using the AFM measurements is shown in Fig. 3(a). The corresponding curves obtained by fitting the data using Hertzian model (refer Supplementary Information) are also shown. The Young's modulus values of different cell lines (MDA MB 231, HL60, MCF7 and HeLa) obtained using our AFM measurements are shown in Fig. 3(b). In each cell line, altogether 20 cells were considered and experiments on each single cell were repeated three-times (thus total $n$=60) for estimating Young's modulus. Young's modulus of cell lines are reported in terms of its mean ±SD as follows; MDAMB231 (1004±100 Pa, $n$=60), HL60 (2675±241 Pa, $n$=60), MCF 7 (3431±377 Pa, $n$=60), HeLa (13532±1623 Pa, $n$=60) under a maximum indentation depth of 1000 nm and indenting load of 30 nN. Standard deviation of the mean value was measured using Student's t-test at the 95% confidence level[47,48]. Young's modulus of cells measured in our AFM experiments is compared with that reported by various researchers in the literature as shown in Table 1. The difference between the Young's modulus values obtained from the present experiments and that reported in literature is attributed to the difference in the protocol including loading rate of AFM probe[26], method of cell immobilization on a substrate, type of probe, fitted model and the depth of indentation on the cells. Thus, we performed AFM measurements on different cells and compared those values by keeping all the above parameters fixed.

From the results, we observe that the HeLa cell line has the highest stiffness, followed by MCF 7 and HL 60 and the MDA MB231 cell line has the least stiffness. It is observed that, the mean value of the Young modulus of MDA MB231 cell line is 65% lower than that of MCF 7 cell line. These observations are in agreement with the previous findings[26,49] that breast cancer cells become softer with malignancy and hence the Young's modulus is reduced significantly. The relative change in the Young's modulus of these breast cancer cell lines (MCF 7 to MDA MB 231) can also be considered as a measure of its invasiveness. From the reported value of Young's modulus, we observed that stiffness of cervical cancer cell line (HeLa) is much higher than the breast cancer cell lines. Experiments are performed for sorting of MDA MB231, MCF 7 and HL60 cell lines from stiffer HeLa cell lines.

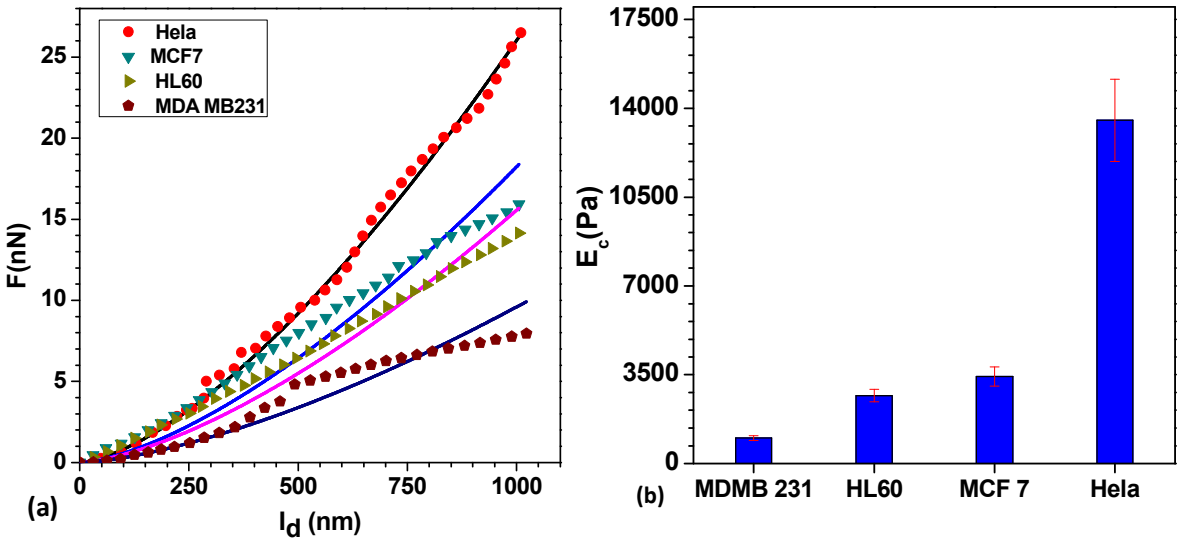


Fig. 3 (a) Force versus indentation curves for different cell lines from AFM experiments (b) Comparison of the Young's modulus of the different cell lines represented as mean ± SD.

View Article Online
DOI: 10.1039/C6RA09099K





Table 1. Comparison of Young's modulus of cells obtained from our AFM measurement with that reported in literature

| Author | Immobilization method | Type of probe | Depth / force of indentation | Cell | Young's Modulus (Pa) |
|---|---|---|---|---|---|
| Rosenbluth et. al (2006)[18] | Using Microwell | Spherical probe | 3 $\mu m$ /800pN | HL 60 | 855± 670 |
| | | | | Jukart | 48±35 |
| | | | | Nuetrophil | 156±87 |
| Dokukin et. al (2013)[50] | Loosely attached | Spherical probe | 1000 nm /10 nN | MCF 7 | 750-1500 |
| Li et. al (2008)[26] | Standard fluid cell | Spherical probe | <400 nm /200 pN | MCF 7 | 310-810 |
| | | | | MCF 10 A | 610-1610 |
| Corbin et. al (2015)[17] | Fixed on a cover slip | Spherical probe | <1000 nm | MDA MB 231 | 856±356 |
| | | | | MCF 7 | 963±277 |
| | | | | MCF 10 A | 1195±397 |
| Zhao et. al (2009)[48] | Fixed on a gloss slide | V-shaped probe | 225 nm | CASKi | 350-470 |
| | | | | CRL 2614 | 1200-1320 |
| Nikkhah et. al (2010)[51] | 3D isotropic silicon microstructure | Spherical probe | <400 nm /0.4 nN | MDA MB231 | 510±350 |
| | | | | MCF 10 A | 1130±840 |
| | | | | HS 68 | 1860±1130 |
| Nikkhah et.al (2011)[52] | Standard fluid cell | Spherical probe | <200 nm | MDA MB231 | 120-620 |
| | | | | MCF 10 A | 1100-1960 |
| Lee et. al (2012) [53] | Fixed on a glass slide | Sharp probe | <500 nm | MDA MB 231 | 500 |
| | | | | MCF 7 | 1300 |
| | | | | MCF 10 A | 2000 |
| Ren et. al (2013) [54] | Seeded on glass slide | Triangular probe | 2nN/ 400 nm | Hela | 12000 (loading rate of 10 Hz) |
| Tomonkova et. al (2012)[55] | Fixed on glass slide | Spherical probe | 325 nm | Hela | 35000 |
| Hayashi et. al (2015)[56] | Seeded on glass slide | Conical probe | <150 nm / 2.5 nN | Hela | 2500 |
| | | | | End1/E6E7 | 5500 |
| Present study | Using Poly-L-Lysine | Spherical probe | 1000 nm / 30 nN) | HL60 | 2675±241 |
| | | | | MDA MB 231 | 1004±100 |
| | | | | MCF 7 | 3431±377 |
| | | | | Hela | 13532±1623 |

### 5.2. Hydrodynamic stretching of different cell lines

In the focusing and spacing control module, the cells focused onto one of the side walls undergo hydrodynamic stretching due to the shear force acting on the cells. The deformation characteristics of the cells is quantified in terms of 'Deformability Index ($D.I.$)', which is defined in our earlier work for droplets[45]. The value of $D.I.$ is zero for cells of much higher stiffness and its value is higher for cells of lower stiffness. Hydrodynamic stretching of MDA MB 231 and HeLa cell lines at a focusing flow rate ratio $f_p$=1.5 (focusing flow rate ratio is the ratio of the sheath fluid flow rate $q$ to the sample fluid flow rate $Q$) is depicted in Fig. 4(a) and (b), respectively. It is observed that MDA MB 231 cells exhibit higher stretching as compared to other cell lines, at the same flow rate ratio. MDA MB 231 cell is the only highly invasive malignant breast cancer cells among the different cell lines studied here.

Since the MDA MB231 cell lines have large Deformability Index ($D.I$), such cells can easily penetrate through tissues and the extracellular matrix (ECM), due to which such cells are highly invasiveness[57]. Hydrodynamic stretching of MCF 7 cell line is lower than that of MDA MB231 cell line. Although MCF 7 cell lines are malignant in nature, they are less invasive as compared to MDA MB231 cell line. The deformability index D.I. of MDA MB 231, HL60, MCF 7 and HeLa cells of different size ratio $\rho_c$ (ratio of the cell diameter to the channel hydraulic diameter) is depicted in Fig. 5. As observed, for a fixed size ratio, *D.I.* of the HeLa cells is found to be much lower as compared to the other cells, which agrees well with the higher stiffness of HeLa cells measured from the AFM measurements. Fitting of the bulk data shows that as the size ratio $\rho_c$ of the cell lines increases, the $D.I.$ of the cell lines also increases linearly, which indicates the larger cells are more deformable. However, in case of MDA MB 231 cells, the *D.I.* increases much faster (with a much steeper slope) with the increase in size ratio $\rho_c$, whereas the *D.I.* of HeLa cells remains almost constant ($D.I.$~ 0.05), irrespective of the size ratio $\rho_c$. The *D.I.* value of the other cell lines are in between that of the MDAMB231 and HeLa cell lines. *D.I.* contrast of the different cells at the focusing module further helps in improving the sorting efficiency (as explained in section 4).

View Article Online
DOI: 10.1039/C6RA09099K




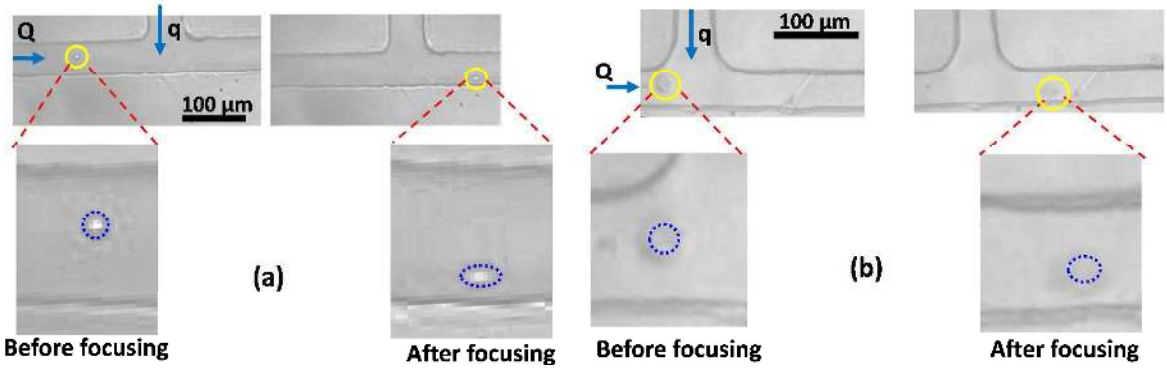


**Fig. 4** Hydrodynamic stretching of (a) MDA MB 231 cells (b) HeLa cells in the focusing and spacing control module at a flow rate ratio of $f_p$=1.5

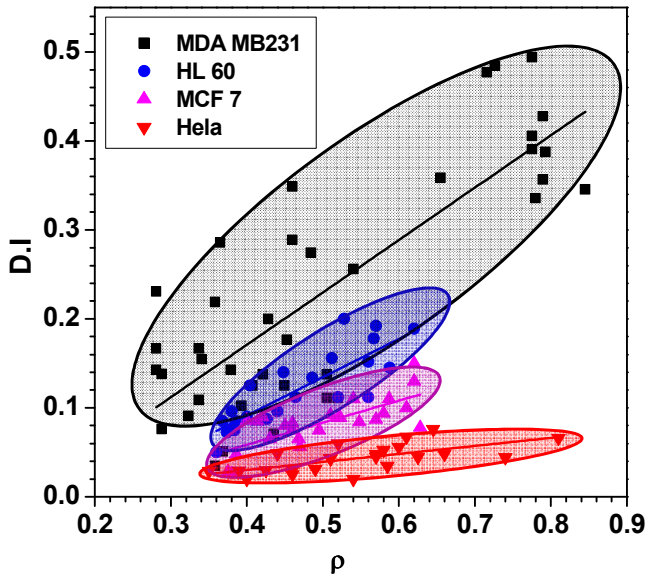


**Fig. 5** Variation in deformability index $D.I.$ of MDA MB 231,MCF 7, HL60 and HeLa cells with different size ratio, at a focusing flow rate ratio of $f_p$=1.5

### 5.3 Induced hydrodynamic resistance of different cell lines

We performed experiments to measure the induced hydrodynamic resistance of different cell lines (MDA MB 231, MCF 7, HL 60 and HeLa) of same size ($25\,\mu m$) to investigate the effect of the cell stiffness (or Young's modulus) on the induced hydrodynamic resistance. The method used for measuring the hydrodynamic resistance of the cells is reported in our earlier work[36]. Induced hydrodynamic resistance of different individual cells (of same size) inside a microchannel is found out and the results are depicted in Fig. 6. As observed, the resistance values are in accordance with the Young's modulus values of the cell lines (shown in Fig. 3b). A higher value of Young's modulus of a cell indicates higher stiffness of the cell membrane and/or higher viscosity of the cytoplasm. A cell line of higher stiffness undergoes less deformation under shear stress inside a microchannel (shown in Fig. 5). In case of a cell of lower stiffness, owing to the higher stretching, the thickness of the thin layer of liquid between the cell membrane and the channel wall is higher. The increased film thickness reduces the viscous dissipation and velocity gradient inside the thin film and this reduces the induced hydrodynamic resistance of more deformable object. Thus, a cell line of higher stiffness would offer higher resistance as compared to a more deformable cell, as observed in Fig. 6. MDA MB 231 cell line is a highly-invasive malignant breast cancer cell line and this malignant transformation process makes the cells more deformable due to the reduction in the amount of organized actin filaments in cytoplasm. It was found that the MDA MB 231 cell line has the least Young's modulus, so it undergoes more deformation (refer Fig. 4) and thus they offers the least hydrodynamic resistance. On the other hand, HeLa cell line has the highest value of Young's modulus, due to which these cells remain

View Article Online
DOI: 10.1039/C6RA09099K



almost undeformed under the shear flow. Thus, the thickness of thin film between the cell and wall is less due to which the HeLa cells offer the maximum hydrodynamic resistance.

We performed a large set of experiments to measure the induced hydrodynamic resistance of cells of different size and stiffness (using different cell lines MDA MB231, MCF 7, HL 60 and HeLa). The hydrodynamic resistance of cells was correlated with the cell size ratio $\rho_c$ and Young's modulus $E_c^*$ as follows,

$$\frac{\Delta R_d}{R} = K\,(E_c^*)^m \rho_c^n \tag{2}$$

where $K$=0.006502, $m$=0.4722 and $n$=2.757. The correlation was found by curve fitting of the experimental data in MATLAB with $R^2$ value of 0.95 and 95% confidence bound, which is later used for the design of the proposed device for sorting of cells of different stiffness (but of same size).

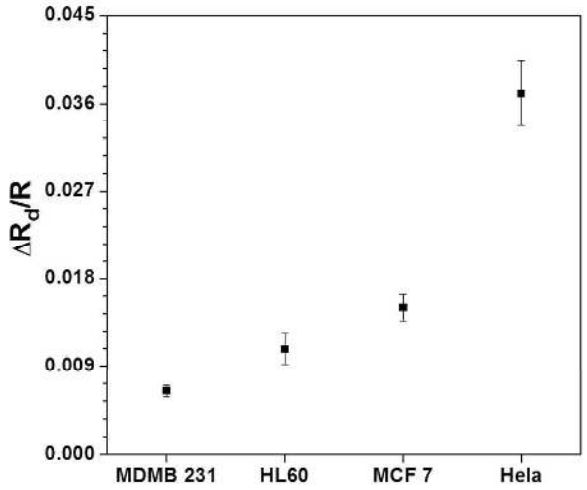


**Fig. 6** Comparison of the hydrodynamic resistance of different cell lines of same size ratio $\rho_c$=0.7

### 5.4 Sorting of cells based on stiffness contrast

#### 5.4.1. Device design, fabrication and setup

The focusing and spacing control module in the upstream of the device focuses the object to one of the side walls and controls the spacing between the objects in the sensing channel by using a sheath fluid. The flow rate ratio $f$ (ratio of the flow rates of the sheath fluid to sample fluid) required to achieve both focusing and spacing control at a time in a device is possible by performing the experiments at a flow rate ratio $f = \max(f_{sc}, f_p)$. (refer Supplementary Information S.5.1). The design of the sorting module used for sorting of objects based on the stiffness contrast is made using the equivalent electrical network of the microchannel presented in Supplementary Information section S.5, in which the resistances $R_i$ and currents $I_i$, respectively, represent the hydrodynamic resistance and flow rates in different segments of the microchannel network. The total resistance across the sensing channel varies due to the variable resistance $\Delta R_c$ (refer Fig. S3 (b)), which depends on stiffness of the object that arrives at the sensing channel. The correlation for hydrodynamic resistance of individual cells $\frac{\Delta R_c}{R}$ with size ratio $\rho_c$ and non-dimensional Young's modulus $E_c^*$ presented in eqn. 2 is used in the equivalent electrical circuit to determine the variable resistance $\Delta R_c$ of cells that arrive at the sensing channel. Using circuit analysis, the equivalent flow rates through the different branches of the microchannel network are obtained and the eqn.S3 presented in Supplementary Information is used to calculate the instantaneous critical stream width $w$. The design of the device for sorting of objects based on the stiffness contrast is made using the analytical model reported in the Supplementary Information section S5. The device of height 20 $\mu m$ using SU8-2025 photoresist was fabricated in PDMS using soft lithography process. The protocol for the fabrication of the device is reported elsewhere[36]. The height of the fabricated microchannel was measured using Scanning Electron Microscopy (SEM), which was found to be 19.3 $\mu m$.

A mixture of any one of the deformable cells (MDA MB231, HL60 or MCF 7) and stiffer cells (HeLa) were used in the sorting experiments. However, for distinguishing the cell lines from each other, the deformable cell line is stained with Rhodamine B (Sigma Aldrich, India) as mentioned in the cell culture protocol in Supplementary Information section S.1.

View Article Online
DOI: 10.1039/C6RA09099K


In order to achieve focusing and spacing control, the cell suspending medium was used as the sheath fluid. Sample and sheath fluid is infused into the device with a syringe pump (TSE systems, Germany). The sorting of cells into the side and straight branch outlets are observed through inverted microscope (Carl Zeiss Axiovert A1,Germany) with fluorescent attachment (HBO 100 illuminator, Germany), coupled with a high-speed camera (Photron FASTCAM SA3) interfaced with PC via Photron FASTCAM viewer software. Finally, the cells were collected at the device outlets and counted using a Haemocytometer (Marienfeld, Germany) to characterize the performance of the device in terms of sorting efficiency.

### 5.4.2 Sorting of cells

We performed experiments to demonstrate sorting of two different cell lines (of same size) based on their stiffness contrast. As discussed earlier, the length of the side branch channel is adjusted to control the side-to-straight branch channel flow rate ratio $r = \frac{Q_{st}}{Q_{si}}$, which in turn controls the critical stream width $w$. The variation of the critical stream width $w$ (obtained from the analytical model reported in Supplementary Information), as a function of the non-dimensional Young's modulus $E_c^*$ of cells, which arrive at the sensing channel, is shown in Fig. 7. In the device presented here, the value of the threshold Young's modulus (explained in section 4) is found to be $E_{ct}^*$ =600. Thus, the present device can be used to sort the deformable cells of stiffness $E_{cd}^*$ <600 from the stiffer cells of $E_{cs}^*$ >600. As discussed, the Young's modulus and hence $\frac{\Delta R_d}{R}$ of HeLa cell lines are much higher than that of MDA MB 231, HL60 and MCF 7 cell lines (of same size). The non-dimensional Young's modulus $E_c^*$ of MDA MB 231, HL60, MCF 7 and HeLa cell lines are approx. 57,153, 197 and 775, respectively. Since, the Young's modulus value of any of these deformable cell lines and the stiffer HeLa cell are on two different sides of the threshold Young's modulus $E_{ct}^*$ =600, the proposed design can be used for sorting of the any of these deformable cells from the HeLa cell present in a mixture based on their stiffness contrast.

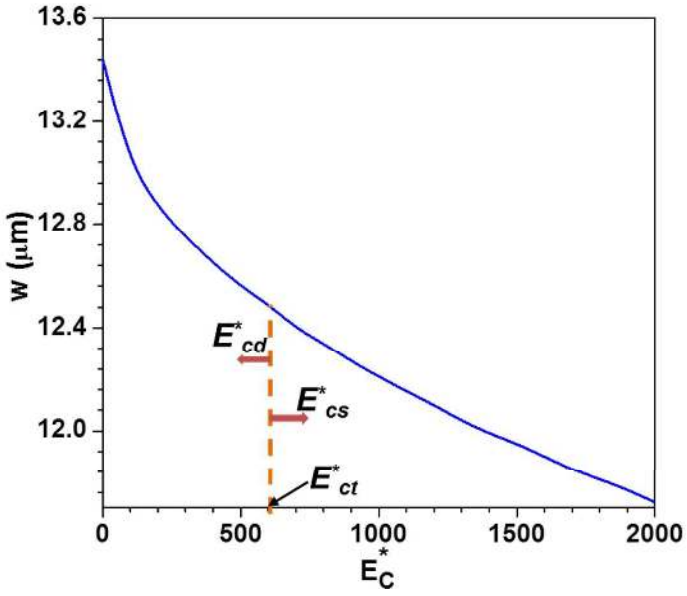


**Fig.7** Variation of instantaneous critical stream width $w$ as a function non-dimensional Young's modulus $E_c^*$

When the deformable cell line enters into the sensing channel, due to lower resistance change, there is a smaller shift in the instantaneous stream width $w$. The dynamic shifting of the critical stream width is demonstrated by observing the position of the streamline at the interface between the sheath and sample fluids as shown in Fig. S4. So, the size of the cell $r_0$ is less than the critical stream width $w_{de}$ thus these deformable cells are sorted into the side branch channel, as shown in Fig.8 (a). In case of HeLa cells, due to higher resistance change, there is a larger shift in $w$. Since the critical stream width $w_{st}$ is lower than $r_0$, these cells are sorted into the main branch channel Fig.14 (b).The cell sorting efficiency was found out by using a mixture of any one of the deformable cell lines and HeLa cells of 25 ±1.0 $\mu m$ size (obtained from FACS).The sorting efficiency is defined as the ratio of the number of cells of one cell line collected at an outlet to the total number of cells of the same size infused into the device within a stipulated time. In order to distinguish the cell lines during the sorting experiments, the deformable cells were stained with Rhodmaine dye and HeLa cells were used without tagging. The sorting efficiency was found to be between 70 and 83% depending on the deformability contrast between the cells to be sorted. The sorting efficiency is higher for two cell lines of large stiffness contrast and lower for that of lower

View Article Online
DOI: 10.1039/C6RA09099K



stiffness contrast. For an example, the sorting efficiency of the device for sorting MDA MB231 from HeLa cells is 83%, whereas sorting of HL60 cells from HeLa cell is found to be 70%. The proposed device can be also used for sorting cells with low stiffness contrast (for example HL60 and MCF 7 cells). This would require a considerable difference between the induced hydrodynamic resistances of the cells when present in the sensing channel. This could be made possible by using sensing channel of smaller width (and bypass channel of even smaller width). In the present work, atmospheric pressure is applied at the device outlets since they are open to atmosphere. The cells with close stiffness contrast can also be sorted by varying the outlet pressures (using external pressure sources).

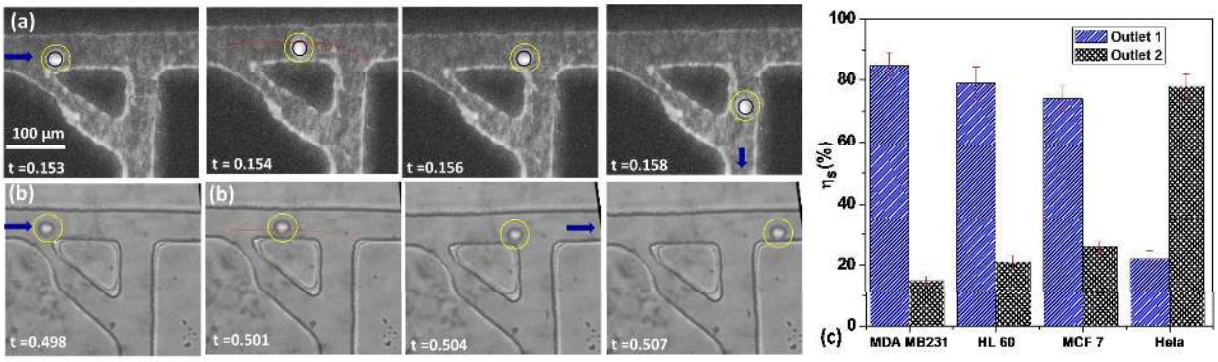


**Fig. 8** Experimental images showing the dynamics of sorting process (a) fluorescent tagged deformable cell (MDMBA 231 cell line) sorted to the side branch (b) HeLa cell of same diameter (25 $\mu m$) sorted to the straight branch, position of dividing streamlines shown (c) Device performance in terms of sorting efficiency to sort other cells from HeLa cells

The sorting module is designed based on hydrodynamic resistance offered by cells as a function of both size and stiffness. Here, we demonstrated the sorting of cells based on stiffness where size of the cells are kept fixed. In our previous work[36], we have correlated the hydrodynamic resistance with cell size and designed a sorting module to sort cells based on size. The proposed device can be used for the sorting of circulating tumour cell from blood using two sorting modules in sequence. First, from the diluted blood (containing CTCs), circulating tumor cells and WBCs (of larger sizes) can be sorted out from other blood components using the size based sorting technique reported in our previous work[36]. The sample thus obtained would contain the mixture of WBCs and CTCs of similar sizes, which can be infused into the present device to sort CTCs from WBCs using the principle of sorting based on stiffness contrast. Hydrodynamic resistance of various blood cell components and CTCs are required for the design of a device to sort CTCs from blood components.

## 6. Conclusion

The stiffness of various cell lines (MDA MB231, HL60, MCF 7 and HeLa) was characterized in terms of Young's modulus $E_c$, Deformability Index $D.I.$ and induced hydrodynamic resistance $\Delta R_C$ and sorting of cells based on stiffness contrast was demonstrated. Young's modulus of different cells are found as follows: MDAMB231 (1004±100 Pa, $n$=60), HL60 (2675±241 Pa, $n$=60), MCF 7 (3431±377 Pa, $n$=60), HeLa (13532±1623 Pa, $n$=60). Among different cells, highly invasive breast cancer cell line MDA MB 231 showed the lowest Young's modulus and cervical cancer cell line HeLa showed the highest Young's modulus. Deformability index ($D.I$) of cell lines was measured by hydrodynamic stretching of cells in a microchannel, which showed that, for a fixed size, the $D.I.$ of the MDA MB 231 cells is much higher as compared to the other cell lines. This observation is in accordance with the literature that the malignant MDA MB231 cell is highly invasive compared to MCF 7 cell, which help them to easily squeeze through ECM structure and tissue to other parts during metastasis. Also, it was observed that $D.I.$ of deformable cells(MDA MB231, HL 60 and HeLa) increases with increase in the size ratio $\rho_c$ but that of stiffer cells (HeLa) is independent of size ratio $\rho_c$. Hydrodynamic resistance of different cells was measured which showed that the hydrodynamic resistance of the stiffer cell (HeLa) is much higher as compared to that of the deformable cell lines and that of MDA MB 231 cells was found to be the lowest. Using a large set of experimental data, the hydrodynamic resistance $\Delta R_c$ is correlated with the size ratio $\rho_c$ and non-dimensional Young's modulus $E_c^*$ of cells, which was further used for the design of the proposed sorting device. Due to the highest stiffness contrast, HeLa and other deformable cell lines of fixed size were selected for the sorting experiments. Sorting experiments were performed using a mixture of any one of the deformable cells (MDA MB 231, HL60 and MCF 7) and stiffer cell (HeLa), both of same size 25 ±1.0 $\mu m$ and the sorting efficiency is found to be in the range 70 and 85% depending on the deformability contrast of cells to be sorted. The sorting efficiency is highest (85%) for a mixture of cells having highest stiffness contrast (i.e. MDA MB 231 and HeLa) and lowest (70%) for that having lowest stiffness contrast (i.e MCF 7 and

View Article Online
DOI: 10.1039/C6RA09099K


HeLa). The proposed device could be potentially used as a diagnostic tool for sorting deformable tumor cells from stiffer leukocytes which have distinct size and stiffness values. Sorting of circulating tumor cell (CTC) from blood would be possible by serially connecting a size based sorting device[36] with the stiffness based sorting device reported here, which is left as the future scope of the work.

**Acknowledgements**

The authors would like to thank the Department of Biotechnology (DBT), India (BT/PR7276/MED/32/267/2012) and for providing the financial support for the project. We also acknowledge CNNP of IIT Madras for supporting the photolithography work. Author would like to thank Mr. Azhar and Prof. T. Pradeep of the Department of Chemistry, IIT Madras and Witec Instruments, Germany for helping with the AFM measurements.

**References**

1 M. Kersaudy-Kerhoas, R. Dhariwal and M. P. Y. Desmulliez, *Nanobiotechnology, IET*, 2008, **2**, 1–13.

2 N. Pamme, *Lab Chip*, 2007, **7**, 1644.

3 P. Sajeesh and A. K. Sen, *Microfluid. Nanofluidics*, 2013, **17**, 1–52.

4 M. Alshareef, M. Nicholas, E. J. Perez, F. Azer, F. Yang, X. Yang and G. Wang, *Biomicrofluidics*, 2013, **7**, 11803.

5 R. A. Harouaka, M. Nisic and S. Y. Zheng, *J Lab Autom.*, 2013, **18**, 1–24.

6 S. Suresh, *Acta Biomater.*, 2007, **3**, 413–438.

7 S. Suresh, J. Spatz, J. P. Mills, a Micoulet, M. Dao, C. T. Lim, M. Beil and T. Seufferlein, *Acta Biomater.*, 2005, **1**, 15–30.

8 A. Vaziri and A. Gopinath, *Nat Mater*, 2008, **7**, 15–23.

9 H. A. Cranston, C. W. Boylan, G. L. Carroll, S. P. Sutera, Williamson, I. Y. Gluzman and D. J. Krogstad, *Sci.* , 1984, **223** , 400–403.

10 J. P. Shelby, J. White, K. Ganesan, P. K. Rathod and D. T. Chiu, *PNAS*, 2003, **100**, 14618–14622.

11 M. Diez-Silva, M. Dao, J. Han, C. T. Lim and S. Suresh, *MRS Bull.*, 2010, **35**, 382–388.

12 J. L. Maciaszek, B. Andemariam and G. Lykotrafitis, *J. Strain Anal. Eng. Des.*, 2011, **46**, 368–379.

13 J. L. Maciaszek and G. Lykotrafitis, *J. Biomech.*, 2011, **44**, 657–661.

14 S. Suresh, J. Spatz, J. P. Mills, A. Micoulet, M. Dao, C. T. Lim, M. Beil and T. Seufferlein, *Acta Biomater.*, 2005, **1**, 15–30.

15 X. Cai, X. Xing, J. Cai, Q. Chen, S. Wu and F. Huang, *Micron*, 2010, **41**, 257–262.

16 O. K. Baskurt, D. Gelmont and H. J. Meiselman, *Am. J. Respir. Crit. Care Med.*, 1998, **157**, 421–7.

17 E. a Corbin, F. Kong, C. T. Lim, W. P. King and R. Bashir, *Lab Chip*, 2015, **15**, 839–47.

18 M. J. Rosenbluth, W. a Lam and D. a Fletcher, *Biophys. J.*, 2006, **90**, 2994–3003.

19 K. Tomankova, P. Kolar, J. Malohlava and H. Kolarova, *Curr. Microsc. Contrib. to Adv. Sci. Technol. (A. Méndez-Vilas, Ed.)*, 2012, 549–554.

20 Y. Zheng, J. Wen, J. Nguyen, M. A. Cachia, C. Wang and Y. Sun, *Sci. Rep.*, 2015, **5**, 1–5.

21 X. Guo, K. Bonin, K. Scarpinato and M. Guthold, *New J. Phys.*, 2014, **16**, 105002.

22 H. W. Hou, Q. S. Li, G. Y. H. Lee, a P. Kumar, C. N. Ong and C. T. Lim, *Biomed. Microdevices*, 2009, **11**, 557–64.

23 S. Byun, S. Son, D. Amodei, N. Cermak, J. Shaw, J. Ho and V. C. Hecht, *PNAS*, 2013, **110**, 7580–7585.

24 R. M. Hochmuth, *J. Biomech.*, 2000, **33**, 15–22.

25 J. L. Alonso and W. H. Goldmann, *Life Sci.*, 2003, **72**, 2553–2560.

26 Q. S. Li, G. Y. H. Lee, C. N. Ong and C. T. Lim, *Biochem. Biophys. Res. Commun.*, 2008, **374**, 609–13.

27 W. Kim and A. Han, in *14th International Conference on Miniaturized Systems for Chemistry and Life Sciences 3 - 7 October 2010, Groningen, The Netherlands*, 2010, pp. 253–255.

28 J. S. Dudani, D. R. Gossett, H. T. K. Tse and D. Di Carlo, *Lab Chip*, 2013, **13**, 3728–34.

View Article Online
DOI: 10.1039/C6RA09099K




29 M. Yamada and M. Seki, *Lab Chip*, 2005, **5**, 1233–1239.

30 J. P. Beech, S. H. Holm, K. Adolfsson and J. O. Tegenfeldt, *Lab Chip*, 2012, **12**, 1048–1051.

31 H. Amini, W. Lee and D. Di Carlo, *Lab Chip*, 2014, **14**, 2739–61.

32 S. C. Hur, N. K. Henderson-MacLennan, E. R. B. McCabe and D. Di Carlo, *Lab Chip*, 2011, **11**, 912–20.

33 J. P. Beech, S. H. Holm, K. Adolfsson and J. O. Tegenfeldt, 2012, 1–7.

34 M. Aurelio and C. Ayala, Massachuesetts Institute of Technology, 2013.

35 M. S. Raafat, M. C. Ayala and R. Karnik, in *14th International Conference on Miniaturized Systems for Chemistry and Life Science*, 2010, pp. 1826–1828.

36 P. Sajeesh, S. Manasi, M. Doble and a K. Sen, *Lab Chip*, 2015, **15**, 3738–48.

37 J. Solon, I. Levental, K. Sengupta, P. C. Georges and P. a Janmey, *Biophys. J.*, 2007, **93**, 4453–61.

38 S. L. Crick and F. C.-P. Yin, *Biomech. Model. Mechanobiol.*, 2007, **6**, 199–210.

39 B. Cappella and G. Dietler, *Surf. Sci. Rep.*, 1999, **34**, 1–104.

40 R. Benitez and J. E. L. Toca-Herrera, *Microsc. Res. Tech.*, 2014, **77**, 947–958.

41 H.-J. Butt, B. Cappella and M. Kappl, *Surf. Sci. Rep.*, 2005, **59**, 1–152.

42 A. L. Weisenhorn, P. Maivald, H.-J. Butt and P. K. Hansma, *Phys. Rev. B*, 1992, **45**, 226–232.

43 L. Sirghi, *Microsc. Sci. Technol. Appl. Educ.*, 2010, **4**, 433–440.

44 H. Hertz, *J. Reine Angew. Math.*, 1882, **92**, 156–171.

45 P. Sajeesh, M. Doble and A. K. Sen, *Biomicrofluidics*, 2014, **8**, 1–23.

46 T. M. Squires and S. R. Quake, *Rev. Mod. Phys.*, 2005, **77**, 977–1026.

47 S. E. Cross, Y.-S. Jin, J. Tondre, R. Wong, J. Rao and J. K. Gimzewski, *Nanotechnology*, 2008, **19**, 1–8.

48 M. Hu, J. Wang, H. Zhao, S. Dong and J. Cai, *J. Biomech.*, 2009, **42**, 1513–9.

49 W. Xu, R. Mezencev, B. Kim, L. Wang, J. McDonald and T. Sulchek, *PLoS One*, 2012, **7**, 1–12.

50 M. E. Dokukin, N. V Guz and I. Sokolov, *Biophys. J.*, 2013, **104**, 2123–31.

51 M. Nikkhah, J. S. Strobl, R. De Vita and M. Agah, *Biomaterials*, 2010, **31**, 4552–61.

52 M. Nikkhah, J. S. Strobl, E. M. Schmelz and M. Agah, *J. Biomech.*, 2011, **44**, 762–766.

53 M. H. Lee, P. H. Wu, J. R. Staunton, R. Ros, G. D. Longmore and D. Wirtz, *Biophys. J.*, 2012, **102**, 2731–2741.

54 J. Ren, S. Yu, N. Gao and Q. Zou, *Phys. Rev. E*, 2013, **88**, 052711.

55 K. Tomankova, P. Kolar, J. Malohlava and H. Kolarova, 2012, 549–554.

56 M. I. Hayashi, K., 2015, **49**, 3.

57 I. Mey, A. Janshoff, J. Rother and H. No, *Open Biol.*, 2014, **4**, 1–7.

View Article Online
DOI: 10.1039/C6RA09099K



This paper reports the characterization and sorting of cells based on stiffness contrast. Cell stiffness is characterized in terms of elastic modulus, deformability index and hydrodynamic resistance. For different cell types, elastic modulus is measured using nanoindentation experiments on AFM and deformability index of cells is measured by hydrodynamic stretching of the cells in a flow focusing microchannel device. Hydrodynamic resistance of cells is obtained by measuring the excess pressure drop across a segment of a microchannel and correlated with cell size $\rho_c$and elastic modulus $E_c^*$ using a large set of experimental data. The highly-invasive malignant breast cancer cells MDA MB 231, non-invasive malignant breast cancer cells MCF 7, human promyelocytic leukaemia cells HL 60 and the cervical cancer cells HeLa are considered in the present study. A microfluidic device with focusing and spacing control for stiffness based sorting of cells is designed and fabricated. Experiments are performed to demonstrate cell sorting and charcterize the device performance in terms of sorting efficiency, which was found to depend on the stiffness contrast. The proposed device has potential to be used as a lab on chip diagnostic tool for sorting of diseased cells from healthy cells based on stiffness contrast.